Journal of Theoretical and Applied Physics (2018) 12:23–31
https://doi.org/10.1007/s40094-018-0276-1

RESEARCH

Theoretical relation between halo current-plasma energy displacement/deformation in EAST

Shahab Ud-Din Khan[1] · Salah Ud-Din Khan[2] · Yuntao Song[3] · Chen Dalong[3]

Received: 20 November 2017 / Accepted: 25 February 2018 / Published online: 28 April 2018

Abstract

In this paper, theoretical model for calculating halo current has been developed. This work attained novelty as no theoretical calculations for halo current has been reported so far. This is the first time to use theoretical approach. The research started by calculating points for plasma energy in terms of poloidal and toroidal magnetic field orientations. While calculating these points, it was extended to calculate halo current and to developed theoretical model. Two cases were considered for analyzing the plasma energy when flows down/upward to the diverter. Poloidal as well as toroidal movement of plasma energy was investigated and mathematical formulations were designed as well. Two conducting points with respect to (R, Z) were calculated for halo current calculations and derivations. However, at first, halo current was established on the outer plate in clockwise direction. The maximum generation of halo current was estimated to be about 0.4 times of the plasma current. A Matlab program has been developed to calculate halo current and plasma energy calculation points. The main objective of the research was to establish theoretical relation with experimental results so as to precautionary evaluate the plasma behavior in any Tokamak.

Keywords Plasma energy · Magnetic field points · Horizontal/vertical forces · Halo current · Mathematical model

List of symbols

A (m^2)	Plasma area
a' (m)	Minor radius
a (m)	Radius of current loop
A_p	Median flow path length
A	Indicates the Plasma tilt positions
B_0 (T)	Initial magnetic field
B_x (T)	Magnetic field in x-direction
B_z (T)	Magnetic field in z-direction
B_θ (T)	Poloidal magnetic field
B (T)	Magnetic field
b (m)	z-axis coordinate of current loop
B_{tor} (T)	Toroidal magnetic field
E (k)	Second type of elliptic integral
I_p (MA)	Total plasma toroidal current
K (m)	Elongation
K (k)	First type of elliptic integral
R' (m)	Major radius
r_p (m)	Plasma radial length
δr_p	Radial kink mode amplitude
Z	z-axis coordinate of calculated point
Δ	Triangularity
ϕ	Magnetic flux
δz_p	Vertical kink mode amplitude
z_p (m)	Plasma vertical length

Electronic supplementary material The online version of this article (https://doi.org/10.1007/s40094-018-0276-1) contains supplementary material, which is available to authorized users.

✉ Shahab Ud-Din Khan
shahab.furqan@gmail.com

Salah Ud-Din Khan
drskhan@ksu.edu.sa

[1] National Tokamak Fusion Program, Pakistan Atomic Energy Commission (PAEC), Islamabad 3329, Pakistan

[2] Sustainable Energy Technologies Center, King Saud University, P.O.Box 800, Riyadh 11421, Kingdom of Saudi Arabia

[3] Institute of Plasma Physics, Chinese Academy of Sciences, P.O.Box 1126, Hefei 230031, Anhui, People's Republic of China

Introduction

During the disruption scenario in plasma, eddy and halo currents were considered to be the most important sources that came out as a result of this phenomenon [1]. The

components which affect primarily are diverter, First Wal (FW) and other main components, because plasma is unstable in vertical displacement. In this scenario, plasma moved upward and downward resulting into plasma disruption, and as a result, halo current has been generated helically. This halo current was produced in SOL component and flows into the vacuum vessel through in-vessel components that may give rise to large force acting on the vessel and in-vessel components [2]. The number of research articles has been published to investigate the halo current in other Tokamak devices such as JET [3], JT-60U [4], and NSTX [5]. Like in Experimental Advanced Superconducting Tokamak (EAST) reactor [6–8], there are some failures of the feedback control in VD event caused by disruption. The EAST reactor is designed by Institute of Plasma Physics, Chinese Academy of Sciences, P.R. China which is considered to be the best superconducting and advanced Tokamak in the world.

Recently, EAST has been updated and had achieved longer pulse generations at high current mode. Main parameters of EAST reactor are given in Table 1 [9].

The EAST has been demonstrated as long-pulsed plasma operations with toroidal field $B_t \leq 3.5$ T and plasma current $I_p \leq 1$ MA [10–12]. The EAST upper diverter has been upgraded with W/Cu plasma facing components (PFCs) with ITER like W-monoblack [13]. The lower diverter has not been upgraded using graphite tiles for the first wall. It has a central dome, but the upper diverter does not equip with it. In addition, an EAST disruption database has been built [14] and is useful for quickly selecting disruptive discharges and their relevant parameters. Nearly, 27% of discharges terminated in a disruption [15].

In this reactor, some sensors have been installed for calculating the halo currents at different locations, as given in Table 2. In these experiments, it was observed that the halo current first spread out on outer baffle plate then moves to dome and finally return back to plasma. At first, we have developed model (2) to calculate magnetic field produced by circular current loop. Furthermore, we considered two cases to analyze the plasma when it flows up/down direction as observed by model (2) calculation data. Second, we have theoretically calculated horizontal/vertical forces connected with model (2). It was observed that generation of halo current was huge and it has strong field at the middle and weak or cancelling effects appear at the sideways positions. Third, during disruption, magnetic field appears at the conducting points consisting of large number of magnetic flux. Therefore, halo current model (18) has been developed using Eqs. (9 and 15) with specific parameters (r_p, z, z_p, u_{shift}, ϕ). A Matlab program has been developed to calculate halo current and magnetic field calculation points. The achievable maximum halo current was about 0.4 times of the plasma current and its maximum TPF values was 0.65 as estimated by set of sensors. EAST halo current is 10 KA for one cassette and total estimation is 400 KA by model (18).

Some of the work that has already been published for halo current is given as under

- Strauss with his team carried out heavy simulation using M3D code for calculating the halo current and plasma disruption conditions [16].
- Long et al. experimentally calculated the values of eddy and halo current in EAST reactor while conducting set of VDE experiments [17].
- Other impressive contributions by Strauss and his team for assessing and simulation of halo current in ITER through VDE instabilities and developed 3D models for plasma disruption conditions [18].
- Fantechi and Crutzen modeled the plasma FW contact under vertical instabilities with a 3D eddy current simulation. The simulation worked for transferring the electric current (halo current) to FW component through VDE [19].

Table 1 Parameters of EAST [9]

Parameters	Values
Major radius	1.7 m
Minor radius	0.4 m
Triangularity	0.6–0.8
Pulse length	1000 s
Plasma current	1 MA
Torroidal field	3.5 T
H&CD	~25 MW
Configuration	Double-null diverter & single null diverter
Elongation(K)	1.6–2
Aspect ratio(R/a)	4.25

Model of magnetic field calculation points for Tokamak

In this research work, a new model for calculating different aspects of Tokamak reactor has been designed. In the recent past, number of work has been published already about the shaping and geometrical description of plasma [20, 21]. One of the important problem is to identify and simulate the plasma shape and control including the numerical calculations on elongated and shaped equilibria [22]. In this paper, a new model was developed on the basis of an applied mathematical approach [23], that is

Table 2 EAST halo diagnostics [17]

Position	Poloidal	Toroidal	Function
Center column	(upper/middle/lower)	–	Measure poloidal halo current
Upper diverter	10	4	Measure halo current through mono block and water cooling tubes
Lower diverter	8 (plate support leg)	4	Halo current in diverter support
	6 (copper plate of dome)	2	Directly measure halo current in dome

$$\begin{aligned} R' &= R_0 + a_{\mathrm{p}}\cos(\theta + \delta\sin\theta) \\ Z' &= Z_0 + k a_{\mathrm{p}}\sin\theta \end{aligned} \tag{1}$$

where "k" is elongation, "δ" is triangularity, "a" is minor radius, and "$R_0^{"}$ is the major radius. Using the algebraic techniques, as the magnetic field is $B = B_X + B_Y$, we obtained B_x and B_z using shape model (1) in energy integral [24]. The calculated points are given as under

$$\begin{aligned} B_x &= B_r\cos\alpha - B_\theta\cos\left(\frac{\pi}{2}-\alpha\right) = B_r\cos\alpha - B_\theta\sin\alpha \\ B_z &= B_r\sin\alpha + B_\theta\sin\left(\frac{\pi}{2}-\alpha\right) = B_r\sin\alpha + B_\theta\cos\alpha. \end{aligned} \tag{2}$$

Magnetic field produced by a circular current loop [25] is

$$\begin{aligned} B_r &= \frac{\mu_0 I}{2\pi r}\frac{z-b}{\left[(a+r)^2+(z-b)^2\right]^{\frac{1}{2}}} \\ &\quad\left[-K(k)+\frac{a^2+r^2+(z-b)^2}{(a-r)^2+(z-b)^2}E(K)\right] \\ B_\theta &= \frac{\mu_0 I}{4\pi r}\frac{1}{\left[a+r)^2+(z-b)^2\right]^{\frac{1}{2}}} \\ &\quad\left[K(k)+\frac{a^2-r^2-(z-b)^2}{(a-r)^2+(z-b)^2}E(K)\right] \\ K(k) &= \int_0^{\pi/2}\frac{\mathrm{d}\alpha}{\sqrt{1-K^2\sin^2\alpha}}, E(k) = \int_0^{\pi/2}\sqrt{1-K^2\sin^2\alpha}\,\mathrm{d}\alpha, \end{aligned} \tag{3}$$

where $R_0 = 1.7$ –1.8, $B_0 = 3.5$T, plasma current $I_{\mathrm{p}} \le 1$ MA.

Plasma orientation and development of halo current

In case of plasma, it was observed that some balancing and unbalancing forces acted upon, like the case of plasma as torus which is very close to outboard wall. At this stage, poloidal field has different radial locations and have variable sideways forces as well. In this case, one side of torus has higher values than other side and poloidal field has different values at different locations.

Case 1 In this case, we considered the plasma at a position (R, Z) from the origin and assumed that during the disruption occurs (Fig. 1), the plasma moves horizontally [26, 27]. The governing equations are given as under

$$F_{\mathrm{h}} = F_1\cos\alpha + F_1\sin\alpha,\ \alpha = 0, 180, 360\ldots \tag{4}$$

$$F_{\mathrm{h}} = F_1\cos\alpha. \tag{5}$$

Since

$$F_{\mathrm{h}} = BI\Delta x\cos\alpha, \tag{6}$$

where

$$\Delta x = \cos\alpha\delta x_{\mathrm{p}}.$$

Therefore

$$F_{\mathrm{h}} = BI_{\mathrm{p}}\left(\cos\alpha\delta x_{\mathrm{p}}\right)\cos\alpha. \tag{7}$$

Since the plasma is in the range of $0 \to 2\pi$, therefore

$$F_{\mathrm{h}} = \int_0^{2\pi} BI_{\mathrm{p}}\cos^2\alpha\delta x_{\mathrm{p}}\mathrm{d}\alpha. \tag{8}$$

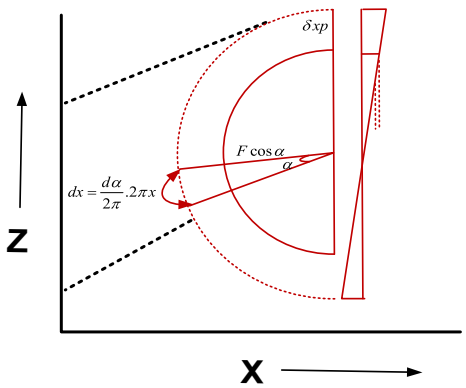

Fig. 1 Plasma orientation (case 1)

$$F_{\mathrm{h}} = BI_{\mathrm{p}}\delta x_{\mathrm{p}} \int_0^{2\pi} \cos^2 \alpha \mathrm{d}\alpha = \pi BI_{\mathrm{p}}\delta x_{\mathrm{p}}. \quad (9)$$

Substitution of Eqs. (2) into (9) gives the changes in magnetic field while applying the horizontal forces on the plasma giving plasma position in different points, as presented in Table 3. For static position, each cross section depends on a, b, r, and z. For one cross section, the peak values of r and z are (± 5.2, ± 4.37); therefore, ($B_{\mathrm{r(max,up)}}$, $B_{\mathrm{r(max,down)}}$) = (0.3918, − 0.3847). Then, the current loop of magnetic field range was (B_x, B_z)$_{\max}$ = (0.3862, 0.1698) for selected degree of cos (alpha) and plasma one cross-sectional area energy was calculated to be 8.0262e + 004. For tilting position, peak values of r and z were (± 5.4, ± 4.17); therefore, ($B_{\mathrm{r(max,up)}}$, $B_{\mathrm{r(max,down)}}$)- = (0.4225, − 0.4247). Hence, the current loop of magnetic field range was (B_x, B_z)$_{\max}$ = (0.4221, 0.1974) for selected degree of cos(alpha) and calculated plasma one cross-sectional area energy was 8.0258e + 004 (see Table 3).

Case 2 In this case, we considered plasma at a position (R, Z) from the origin and assumed that during disruption occurs (Fig. 2), plasma moves vertically downward [26, 27]. The governing equations are given as under

$$F_v = F_2 \cos\beta + F_2 \sin\beta,\ \beta = 90, 270\ldots \quad (10)$$

Then

$$F_v = F_2 \sin\beta. \quad (11)$$

Since

$$F_v = BI\Delta z \sin\beta, \quad (12)$$

Where

$$\Delta z = -\sin\beta\delta z_{\mathrm{p}}.$$

Therefore

$$F_v = BI_{\mathrm{p}}\left(-\sin\beta\delta z_{\mathrm{p}}\right)\sin\beta. \quad (13)$$

Since the plasma is in the range of $0 \rightarrow 2\pi$:

$$F_v = -\int_0^{2\pi} BI_{\mathrm{p}} \sin^2\beta\delta z_{\mathrm{p}}\mathrm{d}\beta. \quad (14)$$

and

$$F_v = -BI_{\mathrm{p}}\delta z_{\mathrm{p}} \int_0^{2\pi} \sin^2\beta \mathrm{d}\beta = -\pi BI_{\mathrm{p}}\delta z_{\mathrm{p}}. \quad (15)$$

Changes in magnetic field can be described by substituting Eq. (2) into Eq. (15) to get the vertical forces applies to the plasma so as to calculates the plasma position at different points. Like in Case-1, each cross section depended upon a, b, r, and z. For one cross section, the peak values of r, z were (± 3.5, ± 2.3); therefore, ($B_{\mathrm{r(max,up)}}$, $B_{\mathrm{r(max,down)}}$) = (0.1865, −0.4652). Then, the current loop of magnetic field range was (B_x, B_z)$_{\max}$ = (0.4637, 0.1995) for selected degree of cos(alpha) and plasma one cross-sectional area energy was 8.0457e + 004. For tilting position, peak values of r and z were (± 3.8, ± 2.5); therefore, ($B_{\mathrm{r(max,up)}}$, $B_{\mathrm{r(max,down)}}$) = (0.2762, − 0.3851). The current loop of magnetic field range was (B_x, B_z)$_{\max}$ = (0.5747, 0.2525) for selected degree of cos(alpha) and the calculated values of plasma one cross-sectional area energy was 8.0484e + 004 (see Table 4).

During VDE, plasma changes the area under vertical and horizontal forces and the magnetic field changes in radial direction at center of plasma with major radius (R), x–z displacement and plasma radial/vertical length (z_{p}, r_{p}). During this plasma change, magnetic field of each point can be calculated by model (2) (vertical and horizontal). The magnetic field appears at the conducting points consisting of large number of magnetic flux, which are given below as

$$\begin{aligned}\phi &= \phi_1 + \phi_2 + \phi_3 + \phi_4 \cdots + \phi_n \\ &= BA_1\cos\phi_1 + BA_2\cos\phi_2 + BA_3\cos\phi_3 \cdots BA_n\cos\phi_n \\ &= B(A_1\cos\phi_1 + A_2\cos\phi_2 + A_3\cos\phi_3 \cdots A_n\cos\phi_n)\end{aligned}$$

$$\phi_{\mathrm{total}} = B\sum_{i=1}^{n} A_i\cos\phi_i. \quad (16)$$

At the conducting points, generation of halo current was huge and it has strong field at the middle and weak forces or cancelling effects appeared at the sideways positions. Due to horizontal and vertical forces, some balancing and unbalancing forces appeared and it was expected that asymmetric plasma positions were along the toroidal coordinates. The poloidal halo current which balances the plasma vertical displacement was toroidally asymmetric. According to the plasma positions, these halo currents have different flow poloidal paths along with the toroidal coordinates. Similarly, due to the asymmetry of poloidal halo currents, the second sideways force occured and the sum of these forces gave sideways balancing forces as well:

$$u(\alpha, \beta) = c\delta x_{\mathrm{p}}.\cos\alpha + d\delta z_{\mathrm{p}}.\sin\beta. \quad (17)$$

The total forces includes horizontal and vertical and the summation of these forces acted upon the plasma VDE direction gives halo current as given below:

$$I_{\mathrm{halo}} = \frac{2}{B}\left[\frac{F_{\mathrm{h}}}{(A_{\mathrm{p}} - z_{\mathrm{p}})u_1} + \frac{F_v}{(A_{\mathrm{p}} - x_{\mathrm{p}})u_2}\right] + \phi_{\mathrm{total}}. \quad (18)$$

During the course of disruption, halo and eddy currents considered to be the main source of electro-mechanical

Table 3 Magnetic field with horizontal displacement by Eqs. (2 and 9)

No.	B_x	B_z	No.	B_x	B_z	No.	B_x	B_z
1	− 0.0277, − 0.0046	0.3162, 0.0523	66	0.2130, − 0.2098	− 0.0053, − 0.0421	132	0.2004, − 0.2151	0.0998, 0.0615
3	− 0.0030−0.0017	0.0347, 0.0193	68	0.1842, − 0.1804	− 0.0140, − 0.0456	134	0.2353, − 0.2441	0.0757, 0.0327
5	− 0.0008, 0.0005	0.0060, − 0.0055	70	0.1390, − 0.1350	− 0.0218, − 0.0453	136	0.2623, − 0.2665	0.0554, 0.0086
7	0.0013, 0.0020	− 0.0151, − 0.0228	72	0.0930, − 0.0889	− 0.0272, − 0.0425	138	0.2810, − 0.2820	0.0378, − 0.0117
9	0.0025, 0.0020	− 0.0284, − 0.0228	74	0.0692, − 0.0645	− 0.0274, − 0.0389	140	0.2909, − 0.2902	0.0223, − 0.0286
11	0.0013, 0.0020	− 0.0151, − 0.0228	76	0.0042, − 0.0409	0.2000, 0.1924	142	0.2903, − 0.2891	0.0083, − 0.0422
13	0.0025, 0.0028	− 0.0284, − 0.0317	78	0.0261−0.0572	0.1698, 0.1598	144	0.2784, − 0.2770	− 0.0042, − 0.0524
15	0.0029,	− 0.0326,	80	0.0692, − 0.0919	0.1279, 0.1122	146	0.2454, − 0.2430	− 0.0162, − 0.0581
16	0.0210, − 0.0674	0.2698, 0.2680	82	0.1110, − 0.1277	0.0990, 0.0773	148	0.2998, − 0.2983	− 0.0558, − 0.0526
18	− 0.0385, − 0.0367	0.1961, 0.1945	84	0.1504, − 0.1618	0.0769, 0.0492	150	0.1986, − 0.2171	0.1501, 0.1073
20	0.0087, − 0.0300	0.1398, 0.1383	86	0.1851, − 0.1918	0.0587, 0.0256	152	0.2340, − 0.2513	0.1147, 0.0685
22	0.0464, − 0.0652	0.1062, 0.1059	88	0.2131, − 0.2161	0.0430, 0.0055	154	0.2668, − 0.2803	0.0866, 0.0366
24	0.0872, − 0.1010	0.0830, 0.0830	90	0.2328, − 0.2334	0.0293, − 0.0115	156	0.0336, − 0.3013	0.0632, 0.0100
26	0.1257, − 0.1353	0.0649, 0.0649	92	0.2431, − 0.2420	0.0169, − 0.0256	158	0.3143, − 0.3156	0.0433, − 0.0125
28	0.1599, − 0.1660	0.0497, 0.0498	94	0.2421, − 0.2401	0.0054, − 0.0366	160	0.3242, − 0.3237	0.0257, − 0.0313
30	0.1879, − 0.1910	0.0365, 0.0365	96	0.2290, − 0.2243	− 0.0162, − 0.0553	162	0.3249, − 0.3246	0.0100, − 0.0468
32	0.2081, − 0.2089	0.0245, 0.0246	98	0.2140, − 0.1820	− 0.1809, − 0.2119	164	0.2914, − 0.2890	− 0.0062, − 0.0548
34	0.2186, − 0.2175	0.0137, 0.0137	100	0.1653, − 0.1391	− 0.1531, − 0.1770	166	0.3086, − 0.3078	− 0.0030, − 0.0564
36	0.2179, − 0.2153	0.0037, 0.0038	102	0.0487, − 0.0806	0.1958, 0.1798	168	0.2806, − 0.2920	0.1320, 0.0757
38	0.2042, − 0.2006	− 0.0054, − 0.0053	104	0.0907, − 0.1153	0.1464, 0.1253	170	0.3125, − 0.3218	0.0994, 0.0403
40	0.1761, − 0.1717	− 0.0136, − 0.0135	106	0.1326, − 0.1512	0.1127, 0.0860	172	0.3380, − 0.3435	0.0724, 0.0107
42	0.1321, − 0.1274	− 0.0206, − 0.0215	108	0.1722, − 0.1851	0.0870, 0.0549	174	0.3570, − 0.3583	0.0494, − 0.0143
44	0.0851, − 0.0804	− 0.0261, − 0.0257	110	0.1574, − 0.1548	0.0663, 0.0290	176	0.3664, − 0.3668	0.0293, − 0.0354
46	− 0.0067, − 0.0298	0.2131, 0.2102	112	0.2071, − 0.2146	0.0486, 0.0071	178	0.3662, − 0.3666	0.0126, − 0.0515
48	0.0121, − 0.0400	0.1510, 0.1449	114	0.2348, − 0.2381	0.0332, − 0.0114	180	0.3363, − 0.3362	0.0102, − 0.0486
50	0.0545, − 0.0753	0.1144, 0.1023	116	0.2541, − 0.2547	0.0194, − 0.0267	182	0.3424, − 0.3464	0.1074, 0.0426
52	0.0959, − 0.1111	0.0890, 0.0706	118	0.2641, − 0.2632	0.0069, − 0.0390	184	0.3862, − 0.3871	0.0816, 0.0109

Table 3 (continued)

No.	B_x	B_z	No.	B_x	B_z	No.	B_x	B_z
54	0.1349, − 0.1453	0.0694, 0.0448	120	0.2635, − 0.2618	− 0.0047, − 0.0477	186	0.3782, − 0.3814	0.0523, − 0.0156
56	0.1693, − 0.1757	0.0532, 0.0230	122	0.2492, − 0.2470	− 0.0151, − 0.0525	188	0.3424, − 0.3464	0.1074, 0.0426
58	0.1974, − 0.2004	0.0390, 0.0042	124	0.2186, − 0.2160	− 0.0210, − 0.0538	190	0.3862, − 0.3871	0.0816, 0.0109
60	0.2174, − 0.2180	0.0264, − 0.0117	126	0.1965, − 0.1862	− 0.0234, − 0.0539	192	0.3782, − 0.3814	0.0523, − 0.0156
62	0.2279, − 0.2267	0.0149, − 0.0249	128	0.1216, − 0.1455	0.1697, 0.1406	194	0.3664, − 0.3668	0.0293, − 0.0354
64	0.2270, − 0.2246	0.0044, − 0.0350	130	0.1613, − 0.1812	0.1298, 0.0964	195	0.3564, − 0.3568	0.0253, − 0.0334

Table 4 Magnetic field with vertical displacement by Eqs. (2 and 15)

No.	B_x	B_z	No.	B_x	B_z	No.	B_x	B_z
1	− 0.0427, − 0.0166	0.6122, 0.1057	66	0.5130, − 0.5097	− 0.0093, − 0.0820	132	0.5004, − 0.5155	0.2098, 0.0918
3	− 0.0080− 0.0077	0.0657, 0.0453	68	0.4842, − 0.4801	− 0.0440, − 0.0854	134	0.5353, − 0.5446	0.0957, 0.0826
5	− 0.00038, 0.0032	0.0090, − 0.0085	70	0.4390, − 0.4352	− 0.0518, − 0.0855	136	0.5623, − 0.5668	0.0954, 0.0156
7	0.0053, 0.0050	− 0.0421, − 0.0418	72	0.2030, − 0.1085	− 0.0572, − 0.0826	138	0.5810, − 0.5819	0.0878, − 0.0412
9	0.0095, 0.0050	− 0.0484, − 0.0418	74	0.0992, − 0.0942	− 0.0574, − 0.0782	140	0.5909, − 0.5900	0.0523, − 0.0585
11	0.0093, 0.0070	− 0.0481, − 0.0418	76	0.0092, − 0.0809	0.5600, 0.4928	142	0.5903, − 0.5890	0.0153, − 0.0829
13	0.0085, 0.0078	− 0.0544, − 0.0507	78	0.0561− 0.0872	0.4698, 0.4595	144	0.5784, − 0.5770	− 0.0142, − 0.0828
15	0.0079,	− 0.0656,	80	0.0992, − 0.2019	0.4279, 0.4124	146	0.5454, − 0.5431	− 0.0462, − 0.0885
16	0.0560, − 0.0954	0.5298, 0.5280	82	0.4110, − 0.4275	0.2090, 0.0972	148	0.5998, − 0.5988	− 0.0858, − 0.0821
18	− 0.0855, − 0.0627	0.4961, 0.4345	84	0.4504, − 0.4618	0.0969, 0.0892	150	0.4986, − 0.5179	0.4501, 0.4072
20	0.0157, − 0.0740	0.4398, 0.4383	86	0.4851, − 0.4918	0.0887, 0.0556	152	0.5340, − 0.5513	0.4147, 0.0989
22	0.0824, − 0.0962	0.4062, 0.4059	88	0.5131, − 0.5162	0.0830, 0.0098	154	0.5668, − 0.5803	0.1066, 0.0665
24	0.1072, − 0.4010	0.1030, 0.1030	90	0.5328, − 0.5334	0.0693, − 0.0415	156	0.0636, − 0.6018	0.0932, 0.0400
26	0.3257, − 0.4353	0.0949, 0.0949	92	0.5431, − 0.5420	0.0469, − 0.0559	158	0.6143, − 0.6156	0.0833, − 0.0426
28	0.3599, − 0.4660	0.0897, 0.0898	94	0.5421, − 0.5400	0.0094, − 0.0766	160	0.6242, − 0.6237	0.0557, − 0.0613
30	0.4879, − 0.4910	0.0765, 0.0765	96	0.5290, − 0.5243	− 0.0462, − 0.0853	162	0.6249, − 0.6245	0.0400, − 0.0765
32	0.4081, − 0.5089	0.0545, 0.0546	98	0.5140, − 0.5820	− 0.4809, − 0.5115	164	0.5914, − 0.5890	− 0.0132, − 0.0848
34	0.5186, − 0.5175	0.0437, 0.0437	100	0.4653, − 0.5391	− 0.4531, − 0.4770	166	0.6086, − 0.6078	− 0.0090, − 0.0864

Table 4 continued

No.	B_x	B_z	No.	B_x	B_z	No.	B_x	B_z
36	0.5179, − 0.5153	0.0087, 0.0079	102	0.0987, − 0.1000	0.4958, 0.4798	168	0.5806, − 0.5920	0.4320, 0.0958
38	0.5042, − 0.5006	− 0.0114, − 0.0103	104	0.2007, − 0.4153	0.4464, 0.4253	170	0.6125, − 0.6219	0.2094, 0.0803
40	0.4761, − 0.4717	− 0.0516, − 0.0435	106	0.4326, − 0.4512	0.4127, 0.1061	172	0.6380, − 0.6435	0.0924, 0.0407
42	0.4321, − 0.4274	− 0.0516, − 0.0515	108	0.4722, − 0.4851	0.1070, 0.0849	174	0.6570, − 0.6583	0.0894, − 0.0445
44	0.1051, − 0.1004	− 0.0561, − 0.0557	110	0.4574, − 0.4542	0.0963, 0.0595	176	0.6664, − 0.6666	0.0593, − 0.0654
46	− 0.0127, − 0.0598	0.5131, 0.5102	112	0.5071, − 0.5146	0.0886, 0.0121	178	0.6662, − 0.6666	0.0426, − 0.0818
48	0.0421, − 0.0800	0.4510, 0.4449	114	0.5348, − 0.5385	0.0632, − 0.0415	180	0.6363, − 0.6362	0.0402, − 0.0886
50	0.0855, − 0.0953	0.4144, 0.4023	116	0.5541, − 0.5547	0.0494, − 0.0567	182	0.6424, − 0.6465	0.4074, 0.0825
52	0.1059, − 0.4111	0.1090, 0.0906	118	0.5641, − 0.5632	0.0109, − 0.0690	184	0.6862, − 0.6871	0.1016, 0.0409
54	0.4549, − 0.4453	0.0994, 0.0848	120	0.5635, − 0.5618	− 0.0117, − 0.0878	186	0.6782, − 0.6816	0.0823, − 0.0457
56	0.4893, − 0.4757	0.0852, 0.0730	122	0.5492, − 0.5470	− 0.0451, − 0.0825	188	0.6424, − 0.6464	0.4074, 0.0826
58	0.4574, − 0.5104	0.0720, 0.0653	124	0.5186, − 0.5160	− 0.0510, − 0.0838	190	0.6862, − 0.6871	0.1016, 0.0400
60	0.5674, − 0.5380	0.0614, − 0.0547	126	0.4965, − 0.4862	− 0.0534, − 0.0839	192	0.6782, − 0.6814	0.0823, − 0.0456
62	0.5479, − 0.5567	0.0429, − 0.0409	128	0.4216, − 0.4455	0.4697, 0.4406	194	0.6664, − 0.6668	0.0593, − 0.0653
64	0.5370, − 0.5546	0.0083, − 0.0590	130	0.4613, − 0.4812	0.4298, 0.2064	195	0.6564, − 0.6568	0.0553, − 0.0665

loads that appeared. Consequently, halo current fraction and toroidal peaking factor (TPF) in vessel components depend upon the halo current density. In MHD simulation problems, plasma model comprises of three regions, namely, core, halo, and resistive wall region integrating plasma to external vacuum magnetic field. In EAST reactor, plasma was inherently unstable against vertical displacement and during upward and downward movement creates disruption along with large halo current generation. In this case, when the plasma flows into the vacuum vessel through in-vessel components, halo current produced large values of $J \times B$ forces acting on the vessel through in-vessel components. The production and movement of halo current is such that it first appeared on the outer plate in clockwise direction and maximum generation of halo current was estimated to be about 0.4 times of the plasma current. Figure 3 shows the evolution of halo current and filament. EAST halo current is 10 KA for one cassette and total 400KA recorded by model (18). In EAST, Rogowski coils have been designed for both the upper and lower diverters to measure the disruption of halo currents. EAST upper diverter was upgraded with a new tungsten diverter consisting of 80 cassettes in the toroidal direction. Four upper diverter, cassettes have been instrumented with a set

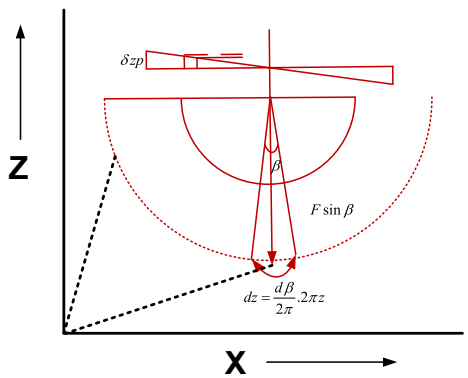

Fig. 2 Plasma orientation (case 2)

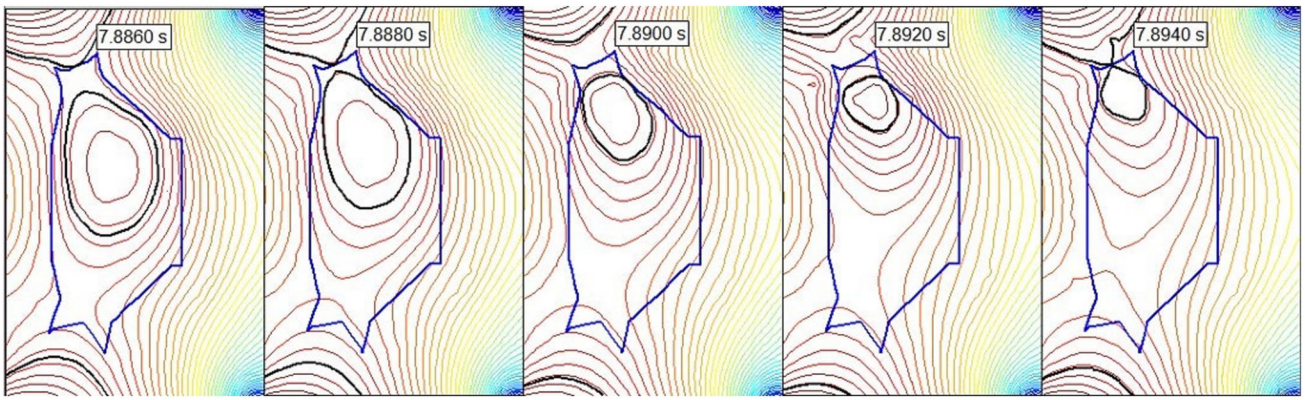

(a)

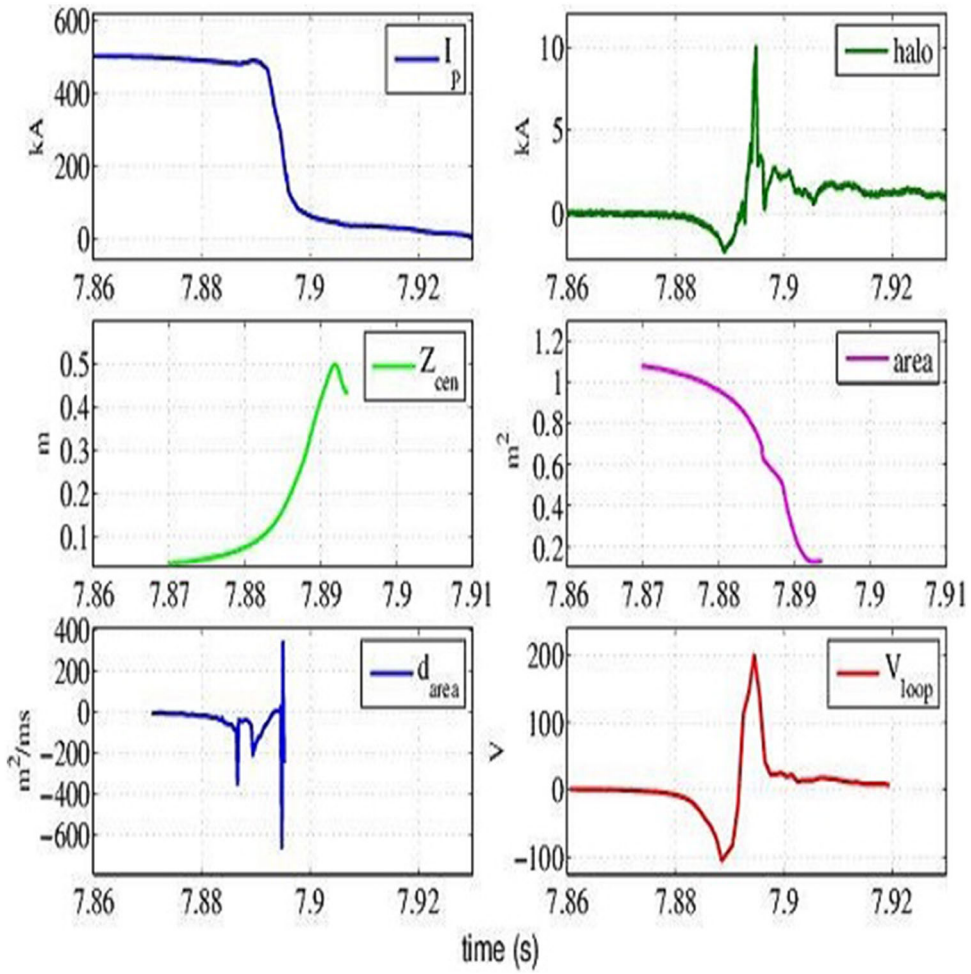

(b)

Fig. 3 Evolution of halo current and filament

of 10 small-cross sections. Rogowski coils to determine where the halo currents enter and exit the diverter, and how much current flows through the water cooling tubes. In this paper, we have successfully performed theoretical investigation between halo current-plasma deformation/ displacement and theoretical calculation of total halo currents as well.

Conclusion

The developed theoretical model calculates plasma cross sections by B_x and B_z magnetic field points and displacement subjected to the start of VDE and magnetic field flux variations. The developed two conducting points give an indication to halo current percentages as well. This model can calculate theoretically halo current during the disruption phases in a very short time. Furthermore, mathematical techniques have been developed successfully which shows the relation between halo currents and plasma displacement/deformation in EAST Tokamak. Computational program has been developed to calculate total halo current and magnetic field calculation points. Theoretical investigation of each cassette has been calculated by model. This model can be subjected to experimental data for other Tokamak devices as well.

Acknowledgements The authors would like to sincerely appreciate the Deanship of Scientific Research at King Saud University for its funding of this research through the Research Group Project No. RGP-255.

References

1. Riccardo, V., et al.: Progress in understanding halo current as JET. Nucl. Fusion **49**, 8 (2012)
2. ITER Physics Expert Group on Disruptions: Plasma Control, MHD and ITER Physics Basis Editors. Nucl. Fusion **49**, 8 (1999)
3. Riccardo, V., Walkerb, S., Nollc, P.: Modelling magnetic forces during asymmetric vertical displacement events in JET. Fusion Eng. Des. **47**(4), 389–402 (2000)
4. Neyatani, Y., Yoshino, R., Nakamura, Y., Sakurai, S.: Characteristics of halo currents in JT-60U. Nucl. Fusion **39**(4), 559 (1999)
5. Gerhardt, S.P.: Dynamics of the disruption halo current toroidal asymmetry in NSTX. Nucl. Fusion **53**, 023005 (2013)
6. Normile, D.: Waiting for ITER. Fusion jocks look EAST. Science. **312**, 992–993 (2006)
7. Wan, B.N.: Recent experiments in the EAST and HT-7 superconducting Tokamaks. Nucl. Fusion **49**, 104011 (2009)
8. Li, J., Wan, B.N.: Recent progress in RF heating and long-pulse experiments on EAST. Nucl. Fusion **51**, 094007 (2011)
9. Wang, X., et al.: Progress of high power and long pulse ECRH system in EAST. Fusion Eng. Des. **96–97**, 181–186 (2015)
10. Wan, B., for the EAST andHT-7 Teams and International Collaborators: Recent experiments in the EAST and HT-7 superconducting tokamaks. Nucl. Fusion **49**, 104011 (2009)
11. Wan, Y.X., Li, L., Weng, P., and EAST team.: Overview progress and future plan of the east project. In: OV/1-1 on 21th IAEA Fusion Energy Conference. Chengdu. China. (2006)
12. Li, J., et al.: A long-pulse high-confinement plasma regime in the Experimental Advanced Superconducting Tokamak. Nat. Phys. 9. 817. 2013
13. Li, J., et al.: Plasma facing components for the Experimental Advanced Superconducting Tokamak and CFETR. Phys. Scr. **T159**, 014001 (2014)
14. Granetz, R.S., et al.: 7th US-PRC Magnetic Fusion Collaboration Workshop. 28. http://www.swip.ac.cn/mfcw2014/7th%20US-PRC%20MFC%20abstracts.pdf#page=29.2014
15. Long, C.D., et al.: Characterization of plasma current quench during disruption in EAST tokamak. Chin. Phys. B **24**, 025205 (2015)
16. Strauss, H.R. et al.: Halo current and resistive wall simulations of ITER. 1-7.TH/2-2
17. Long, C.D. et al.: Observation and analysis of halo current in EAST. Chin Phys B. **23**, 065205 (2014)
18. Strauss, H.R.: Non-linear MHD halo current simulations, TH/2-3
19. Fabtechi, S., Crutzen, Y.: Modelling and analysis of plasma-first wall contact during vertical instabilities in next-step tokamaks with a 3D eddy current code. In: Fusion Technology 1996. Proceedings of the 19th Symposium on Fusion Technology, Lisbon, Portugal, 16–20 September 1996, pp. 727–730. Elsevier, Amsterdam (1997)
20. Long, C.D., et al.: Halo current diagnostic system of experimental advanced superconducting tokamak. Rev. Sci. Instrum. **86**, 103506 (2015)
21. Pironti, A., et al.: Optimal choice of the geometrical descriptors for tokamak plasma shape control. Fusion Eng. Des. **43**, 115–127 (1998)
22. Kurihara, K.: A new shape reproduction method based on the Cauchy-condition surface for real-time Tokamak reactor control. Fusion Eng. Des. **51–52**, 1049–1057 (2000)
23. Hofinann, F., et al.: Equilibrium and axisymmetric stability of the proposed TCV Tokamak. 14th Symposium on Fusion Technology. Fusion Technol. **1**, 687–692 (1986)
24. Wesson, J.: Tokamaks. Oxford Univ Press, Oxford (2011)
25. Yuntao, S., Wu, W., Du, S.: Tokamak engineering mechanics. Mechanical Engineering Series. Springer, Berlin (2014). ISBN: 978-3-642-39574-1
26. Bachmann, C.: Asymmetric forces on the ITER plasma in kink mode in subsequent halo currents in the VV. ITER_D_28P25D v1.0. (2015)
27. Forces on the ITER Vacuum Vessel due to the Plasma in Kink Mode during a VDEIII with Slow Current Quench, ITER_D_26RLC9